

## Design, dynamic docking, synthesis, and *in vitro* validation of a novel DNA gyrase B inhibitor

Akhila Pudipeddi, Sahana Vasudevan, Karthi Shanmugam, Suma Mohan S, Pothiappan Vairaprakash, Prasanna Neelakantan, Alex Stanley Balraj & Adline Princy Solomon

To cite this article: Akhila Pudipeddi, Sahana Vasudevan, Karthi Shanmugam, Suma Mohan S, Pothiappan Vairaprakash, Prasanna Neelakantan, Alex Stanley Balraj & Adline Princy Solomon (2022): Design, dynamic docking, synthesis, and *in vitro* validation of a novel DNA gyrase B inhibitor, Journal of Biomolecular Structure and Dynamics, DOI: [10.1080/07391102.2022.2107073](https://doi.org/10.1080/07391102.2022.2107073)

To link to this article: <https://doi.org/10.1080/07391102.2022.2107073>



View supplementary material [↗](#)



Published online: 04 Aug 2022.



Submit your article to this journal [↗](#)



Article views: 86




View related articles [↗](#)



View Crossmark data [↗](#)



## Design, dynamic docking, synthesis, and *in vitro* validation of a novel DNA gyrase B inhibitor

Akhila Pudipeddi<sup>a,b</sup> , Sahana Vasudevan<sup>a</sup> , Karthi Shanmugam<sup>a,c</sup> , Suma Mohan S<sup>c</sup> , Pothiappan Vairaprakash<sup>d</sup> , Prasanna Neelakantan<sup>b</sup> , Alex Stanley Balraj<sup>a,c</sup>  and Adline Princy Solomon<sup>a</sup> 

<sup>a</sup>Quorum Sensing Laboratory, Centre of Research in Infectious Diseases, School of Chemical and Biotechnology, SASTRA Deemed to be University, Thanjavur, India; <sup>b</sup>Faculty of Dentistry, The University of Hong Kong, Pok Fu Lam, Hong Kong; <sup>c</sup>Department of Bioinformatics, School of Chemical & Biotechnology, SASTRA Deemed to be University, Thanjavur, India; <sup>d</sup>Department of Chemistry, School of Chemical & Biotechnology, SASTRA Deemed to be University, Thanjavur, India

Communicated by Ramaswamy H. Sarma

### ABSTRACT

Methicillin-resistant *Staphylococcus aureus* (MRSA) and vancomycin-intermediate-resistant *Staphylococcus aureus* (VRSA) are among the WHO's high priority pathogens. Among these two, MRSA is the most globally documented pathogen that necessitates the pressing demand for new classes of anti-MRSA drugs. Bacterial gyrase targeted therapeutics are unique strategies to overcome cross-resistance as they are present only in bacteria and absent in higher eukaryotes. The GyrB subunit is essential for the catalytic functions of the bacterial enzyme DNA Gyrase, thereby constituting a promising druggable target. The current study performed a structure-based virtual screening to designing GyrB target-specific candidate molecules. The *de novo* ligand design of novel hit molecules was performed using a rhodanine scaffold. Through a systematic *in silico* screening process, the hit molecules were screened for their synthetic accessibility, drug-likeness and pharmacokinetics properties in addition to its target specific interactions. Of the 374 hit molecules obtained through *de novo* ligand design, qsl-304 emerged as the most promising ligand. The molecular dynamic simulation studies confirmed the stable interaction between the key residues and qsl-304. qsl-304 was synthesized through a one-step chemical synthesis procedure, and the *in vitro* activity was proven, with an IC<sub>50</sub> of 31.23 µg/mL against the novobiocin resistant clinical isolate, *Staphylococcus aureus* sa-P2003. Further studies on time-kill kinetics showed the bacteriostatic nature with the diminished recurrence of resistance. The on-target gyrB inhibition further proved the efficacy of qsl-304.

### ARTICLE HISTORY

Received 11 October 2021  
Accepted 23 July 2022

### KEYWORDS

*Staphylococcus aureus*;  
Novobiocin; Rhodanine; *De novo*-based drug design; gyrase inhibitor; antibacterial resistance


## 1. Introduction

Multidrug resistance is a major global public health issue caused due to the indiscriminate use of broad-spectrum antimicrobials and counterfeit antimicrobials (Mattingly et al., 2020). Such falsified and substandard antimicrobials may contain toxic doses of dangerous ingredients, compromise the treatment of chronic and infectious diseases, cause disease progression and drug resistance, and increase the mortality rate (Johnston & Holt, 2014). Recent hospital-based surveillance reports suggest the emergence of a resistant group of nosocomial pathogens comprising *Enterococcus faecium*, *Staphylococcus aureus*, *Klebsiella pneumoniae*, *Acinetobacter baumannii*, *Pseudomonas aeruginosa*, and *Enterobacter* species (ESKAPE pathogens) that have diminished the efficacy of many frontline antibacterial agents, which will result in a global financial burden of ~100 trillion USD by 2050 (Tomašić & Mašić, 2014; Rice, 2008; Bush & Jacoby, 2010; Savage et al., 2016).

According to the Centre for Disease Control and Prevention (CDC), the ESKAPE pathogen, Methicillin resistant-*S. aureus* is a crucial player in causing severe community-acquired and hospital-related infections (Lakhundi & Zhang, 2018; Ventola, 2015). The widespread usage of antibiotics, acquisition and accumulation of resistance-conferring alleles have resulted in the emergence of MRSA strains to develop cross-resistance to vancomycin (VAN), trimethoprim-sulfamethoxazole, β-lactams, tetracycline, clindamycin, quinolones, and aminoglycosides (Livermore, 2000; Bozdogan et al., 2003; Rice, 2006). Antibiotics that inhibit multiple targets tend to exhibit lower spontaneous-resistance frequencies, and their antibacterial activity is less affected by individual, target-based mutations. This potentially delays the emergence of high-level resistance in pathogens, a major cause of treatment failure (Sareena & Vasu, 2020). The resistance of MRSA to already existing antibacterial drugs might be due to the Staphylococcal Chromosomal Cassette gene

**CONTACT** Adline Princy Solomon  [adlineprinzy@sastra.ac.in](mailto:adlineprinzy@sastra.ac.in)  Quorum Sensing Laboratory, Centre of Research in Infectious Diseases, School of Chemical and Biotechnology, SASTRA Deemed to be University, Thanjavur, 613401, India

\*Contributed equally to the manuscript.

 Supplemental data for this article can be accessed online at <http://dx.doi.org/10.1080/07391102.2022.2107073>

© 2022 Informa UK Limited, trading as Taylor & Francis Group

mec (SCCmec) and Panton-Valentine Leukocidine (PVL) toxin gene that enhances bacterial virulence (Ray et al., 2011)

There is a pressing demand for new anti-MRSA drugs to avoid cross-resistance with currently used antibacterial drug classes and meet the inadequacies of current anti-MRSA therapies. Indeed, the need for designing anti-MRSA drugs may discover novel mechanisms of action or focus on previously unexploited binding sites on existing targets or develop novel scaffolds without developing cross-resistance (Basarab et al., 2014; Mani et al., 2006). In this accord, bacterial gyrase targeted therapeutics are unique since it is the universal enzyme required for bacterial survival and is absent in higher eukaryotes (Collin et al., 2011). DNA gyrase (gyrase), a member of bacterial topoisomerases, is known to control the DNA dependent processes by introducing transient breaks to both DNA strands (Bax et al., 2019), in addition to relieving the torsional tension, by introducing negative supercoils to the DNA molecule (Hurley et al., 2017). DNA gyrase is a heterotetrameric protein composed of two GyrA subunits where the DNA cleavage site is located. Two GyrB subunits provide the energy necessary for the enzyme's catalytic function through ATP hydrolysis (Savage et al., 2016). Therefore, drugs that target bacterial topoisomerases act by two main mechanisms, either by stabilizing the complex between the DNA molecule and the GyrA active site of the enzyme (e.g. quinolones) or by inhibiting the ATPase activity of the GyrB subunit (e.g. aminocoumarin class of inhibitors) (Durcik et al., 2018). Recently Tiz et al., have tested N-Phenylpyrrolamide derivatives that interact with the ATP binding site of DNA gyrase and have reported that the most potent compound (quinolone derivative) has inhibited the growth of *S. aureus* (MIC = 0.78 mM), MRSA (MIC = 2.5 mM) and extremely drug-resistant strain of *S. aureus* (MRSA VISA) with a MIC 2.5 mM. Even though the compound has exhibited excellent MIC against many organisms, its antibacterial activity couldn't be explained through the targeted activity of the compound, and further studies are required to confirm its mode of action (Tiz et al., 2019).

Linezolid (LZD), which retains its activity against resistant Gram-positive strains, is available in both intravenous and oral formulations, but the dose and therapeutic duration of LZD was not enough to eradicate MRSA in patients (Kohn et al., 2007; Purnapatre et al., 2018). Tedizolid, another anti-MRSA antibacterial that is available again in both intravenous and oral formulations, is used to treat acute bacterial skin and skin structure infections (ABSSSIs). However, there are safety and efficacy concerns over tedizolid in patients with neutropenia (Wong & Rab, 2014; Purnapatre et al., 2018). Hence, Novobiocin, a representative of the natural aminocoumarins, was the only clinically-approved potent inhibitor of GyrB with inhibition (Ki) and binding (Kd) constants in the low nanomolar range (7–15 nM) (Chopra et al., 2012), until recently, wherein the United States Food and Drug Administration (FDA) withdrew its approval due to issues of toxicity and poor physicochemical properties, urging the discovery of an improved successor to novobiocin (Bisacchi & Manchester, 2015). The discovery of new drugs with novel scaffolds targeting the ATP binding site of GyrB without any

cross-resistance and toxicity issues will complement the failure of novobiocin (Durcik et al., 2018). Sareena et al. suggest that the aminocoumarins are stronger and more advantageous than novobiocin and clorobiocin, can act against both antibiotic sensitive and resistant strains of *S. aureus* and have investigated the effect of a compound (4-DPA3IC) that contributes to overcoming the drug resistance problem of the pathogen and paves a path to validate the efficacy of plant drug formulations used in traditional medicine (Sareena & Vasu, 2020). However, several reports also suggest that heterocyclic compounds with rhodanine scaffolds are known to inhibit several pharmaceutical targets from demonstrating enhanced antimicrobial activity (Maddila et al., 2020). 3, 5-disubstituted rhodanine derivatives inhibited the *S. aureus* supercoiling activity by targeting the GyrB ATPase function (Werner et al., 2014). Other rhodanine derivatives such as 5-(2-hydroxybenzylidene) have shown moderate antibacterial activity, reported as GyrB inhibitor (Brvar et al., 2012), phenylalanine derived (z)-5-arylmethylidene rhodamine (Patel et al., 2013), 2-(5-(3,4-Dichlorobenzylidene)-4-oxo-2-thioxothiazolidin-3-yl)-3-phenylpropanoic acid and 2-(5-(3-Phenoxybenzylidene)-4-oxo-2-thioxothiazolidin-3-yl)-3-phenylpropanoic acid (Hardej et al., 2010) have shown significant anti-MRSA activity, can be used for the treatment of gram-positive MRSA (AbdelKhalek et al., 2016). Thus, compounds with rhodanine scaffold were observed to show a broad spectrum of pharmacological activity (Tomai & Mai, 2009), and further structural modification may enable them as potent, selective drugs.

In this regard, the current study is aimed to identify potent compounds that target the ATP binding site through a systematic virtual screening process. We have extended our search to find efficient GyrB-targeted inhibitors using *de novo*-based ligand design. An insight of recent work on NMR-fragment-based binding study against the co-crystallized full-length *S. aureus* GyrB ligand (Mesleh et al., 2016) was taken to optimize the target-specific hit molecules with rhodanine scaffold using LigBuilder. The bioavailability and pharmacokinetics of the top-hit ligands were further scored based on ADMET properties, and we then evaluated the biological efficacy against MRSA *in vitro*.

## 2. Materials and methods

### 2.1. *In silico* studies

#### 2.1.1. Protein selection

The current computational studies were done with the crystal structure of *S. aureus* GyrB complexed with a fragment (indolinone derivative), PDB ID: 5CPH. The considered protein, GyrB, consists of two chains (homodimer), A and B, having 212 amino acids with a resolution of 1.20 Å. Based on the resolution, A chain of this protein structure was chosen for further computational studies.

#### 2.1.2. *De novo* ligand design

A structure-based drug design methodology termed *de novo* ligand design was carried out using LigBuilder (Wang et al.,

2000). *De novo* design is a successful ligand design method where the novel ligands are built stepwise considering the protein binding pocket constraints. The unique advantage of this method is the generation of molecules based on the target protein, which is unique and not available in any other small molecule databases. LigBuilder is one of the acclaimed *de novo* tools which builds the ligands from the library of organic molecules having 60 fragments valuable to the drug design process. There are two modules of "growing" and "linking" to build ligands controlled by genetic algorithms. The current study was designed based on the "grow" concept between the two approaches. Here, the seed structure plays an important role and is the starting point of hit optimization's whole *de novo* design. Rhodanine scaffold was designated as the seed structure for the hit optimization process. All the molecules generated out of the *de novo* drug design will have the structural framework of rhodanine. Another requirement is the pre-docked protein-ligand complex for the program to locate the binding pocket. As there was no co-crystallized rhodamine-GyrB complex structure in the protein data bank, we docked rhodanine moiety in the binding pocket of *S. aureus* GyrB (PDB ID: 5CPH) and used it for pocket exploration. The "building" of the molecule from the rhodanine core was from the two hydrogen atoms at the C5 position. The next step is the mutation operation, where the generated molecules are improved for their ligand-binding affinity. The building up process is further amplified using genetic algorithms. Finally, *de novo* designed molecules are obtained.

### 2.1.3. Synthetic accessibility score

One of the significant limitations of the *de novo* ligand design is the synthetic feasibility. Thus, the newly developed *de novo* compounds were subject to synthetic accessibility to overcome this barrier. SYBA (SYnthetic Bayesian Accessibility) was used to classify the *de novo* designed molecules as easy – (ES) and hard-to – synthesize (HS) organic compounds based on the analysis of the individual substructures of the given hit molecules (Voršilák et al., 2020). SYBA is the latest improved version of SAScore and SCScore with ES molecules trained with the molecules of ZINC15 database and HS molecules from Nonpher methodology. SYBA works on Bernoulli naïve Bayes classifiers where each compound is fragmented into substructures, and each fragment is scored. The individual substructures score is added to get the final SYBA score. The analysis is based on the score obtained by Bayesian analysis. The positive scores imply ES and negative scores, HS. SYBA is publicly available at <https://github.com/lich-uct/syba> under the GNU General Public License.

### 2.1.4. Protein preparation

Schrödinger's Protein Preparation Wizard (Sastry et al., 2013) is used for the preparation of the three-dimensional structure of the ATP binding domain of *S. aureus* GyrB complexed with a (3E)-3-(pyridin-3-ylmethylidene)-1,3-dihydro-2H-indol-2-one inhibitor (PDB ID: 5CPH). The protein preparation workflow briefly includes adding missing hydrogen atoms,

enumerating bond orders to HET groups, removing co-crystallized water molecules (non-structural), determining the most likely protonation state, correcting potentially transposed heavy atoms, and optimizing the proteins hydrogen bond network. Finally, the protein was subjected to a restrained minimization that allows hydrogen atoms to be freely minimized while allowing for sufficient heavy atom movement to relax strained bonds, angles, and clashes.

### 2.1.5. Receptor grid generation

The recognition of the active site or the binding site of the target structure accurately is a critical step in drug designing through computational docking of the novel chemical moieties. Schrödinger GLIDE (Grid-based ligand docking with energetics) docking protocol generates a grid around the protein's active site for ligand docking (Friesner et al., 2006). The shape and properties of the receptor are represented on a grid by several different fields that provide progressively more accurate scoring of the ligand poses. The grid box was generated using a receptor grid generation panel. The grid box is positioned on the centroid of the co-crystallized ATP binding domain inhibitor (3E)-3-(pyridin-3-ylmethylidene)-1,3-dihydro-2H-indol-2-one. The ATP binding pocket of GyrB is well characterized and reported. Hence a manual check was done to ensure that the generated grid encloses all the essential amino acids of the GyrB ATP binding site (D81, R84, G50, R144 and HOH427). The protein atoms were fixed within the default parameters of the radii of Vander Waal's scaling factor of 1 Å with a partial charge cut-off of 0.25 Å using OPLS3e force field, and 20 Å docked ligand length. The dimensions of the grid box and receptor setup were  $x = 22 \text{ Å}$ ,  $y = 22 \text{ Å}$ ,  $z = 22 \text{ Å}$  and  $x = 64 \text{ Å}$ ,  $y = 64 \text{ Å}$ ,  $z = 64 \text{ Å}$  during the docking study, respectively, with a grid space of 1 Å.

### 2.1.6. Ligand preparation

An accurate 2D to the 3D conversion of ligand molecules is a crucial precursor to computational docking studies. The 374 novel ligands designed through the LigBuilder algorithm were prepared using the LigPrep module implemented in Schrödinger (Schrödinger Release 2020-4: LigPrep, Schrödinger, LLC, New York, NY, 2020.). LigPrep generates accurate, energy minimized 3D molecular structure using OPLS3e force field. It also applies sophisticated rules to correct Lewis structures and eliminate mistakes in ligands to reduce downstream computational errors. LigPrep expands tautomeric and ionization states, ring conformations, and stereoisomers to produce structural diversity from a single input structure.

### 2.1.7. High throughput virtual screening

The prepared 374 molecules generated by LigBuilder were taken further for high throughput virtual screening (HTVS) against a target protein (PDB ID: 5CPH). The ligands were docked using Glide (Flexible mode) to evaluate the binding



modes. Glide extra precision docking was carried out for all the 374 molecules (Friesner et al., 2006).

### 2.1.8. Lipinski's and Veber's rules

Schrodinger Qikprop (Schrödinger, LLC, New York, NY, 2020) was used for a different level of filtering to identify the molecules having drug-likeness using Lipinski's Rule of Five (Hydrophobicity less than 5, molecular weight less than 500 Da, hydrogen bond (HB) donor and acceptor less than 5 and 10 respectively). In addition to that, the hit molecules were assessed for Veber's rule having rotatable bonds <10 and polar surface area < 140 Å were also taken for the screening process.

### 2.1.9. ADMET prediction

The molecules that did not violate Lipinski's and Veber's rules were further assessed for the ADMET properties using Discovery Studio. ADME (Absorption, Distribution, Metabolism and Excretion) assessment is required to filter the hit molecules with desirable pharmacokinetic properties. The ADME descriptors include aqueous solubility, Blood-brain barrier penetration, Cytochrome P450 2d6 inhibition, Hepatotoxicity, Human Intestinal absorption, and Plasma protein binding. The hit molecule(s) which satisfy the above properties are taken for *in vitro* analyses.

### 2.1.10. Molecular dynamics simulation studies

MD simulation studies of the docked complex, GyrB-qs1304 were done using the Desmond (v5.6) package (Bowers et al., 2006). System Builder was used for the preparation of the simulation system using an orthorhombic box shape with a 10 Å buffer distance with the solute. TIP4P water model was used, and counter ions were added to neutralize the system. Additional ions were added to obtain the physiological salt concentration of 0.15 M. The simulation system was relaxed before the production run using the default relaxation protocol available with desmond. A 300 ns MD simulation for GyrB:qs1-304 complex and a 50 ns MD simulation for GyrB:Novobiocin complex were carried out using the OPLS2005 force field. The simulation was performed in the NPT ensemble using the Nose-Hoover chain thermostat (300 K) and Martyna-Tobias-Klein barostat (1 atm). The simulation interaction diagram analyzed the MD simulation trajectory (Schrödinger, LLC, New York, NY, United States, 2020). The average binding free energy for both complex trajectories based on MM-GBSA was calculated using the thermal\_mmgb.py script with a step size of 100 (Schrödinger, LLC, New York, NY, United States, 2020).

## 2.2. Synthesis of (Z)-(5-((4-oxo-2-thioxothiazolidin-5-ylidene)methyl)furan-2-yl)methyl acetate

A suspension of rhodanine (18.0 mmol, 2.34 g) and 5-hydroxymethylfurfural (19.4 mmol, 2.45 g) in glacial acetic acid (19.4 mL) was heated to 80 °C for complete dissolution (Rosatella et al., 2011). The resulting solution was treated

with sodium acetate (77.8 mmol, 6.37 g) at 80 °C for 15 h. Completion of the reaction was monitored by TLC analysis using a solvent mixture containing hexane and ethyl acetate (1:1, v/v) as an eluent. Then the reaction mixture was treated with water (50 mL) and extracted using ethyl acetate (3 × 30 mL). The combined organic extract was dried over sodium sulphate and filtered. The solvent was removed by rotary evaporation, and the resulting residue was purified by column chromatography [silica, ethyl acetate: hexane (1:9)] to obtain the compound (Z)-(5-((4-oxo-2-thioxothiazolidin-5-ylidene) methyl) furan-2-yl)methylacetate (indicated as qsl-304, herein) as a yellow solid. Further, the compound qsl-304 was completely characterized using NMR spectroscopy and Mass spectrometry. <sup>1</sup>H NMR confirmed the structural details of the synthesized compound. The peak assignment of the spectrum are as follows: <sup>1</sup>H NMR (300 MHz, CDCl<sub>3</sub>) δ 2.06 (s, 3H), 5.05 (s, 2H), 6.51 (d, *J* = 2.1 Hz, 1H), 6.73 (d, *J* = 1.8 Hz, 1H), 7.27 (d, *J* = 2.7 Hz, 1H); <sup>13</sup>C NMR (75 MHz, CDCl<sub>3</sub>) δ 20.7, 57.9, 113.8, 117.6, 119.3, 124.3, 150.1, 154.2, 169.4, 170.8, 195.9; LCMS obsd 284.0053, calcd 284.0056 (M + H; M = C<sub>11</sub>H<sub>9</sub>NO<sub>4</sub>S<sub>2</sub>).

## 2.3. In vitro assays

### 2.3.1. Antibiotic and test compound preparation

The antibiotic novobiocin was obtained as a DMSO-soluble powder with 96% purity (Sigma-Aldrich (St Louis, MO, USA)). The stock solution of the test compound, qsl-304 was prepared in 1% DMSO. The final concentration of DMSO was maintained as <0.5%.

### 2.3.2. Bacterial strains and culture maintenance

The reference strain, *S. aureus* ATCC43300 was purchased from the American Type Culture Collection (ATCC; Manassas, VA). The clinical isolates, Sa-P1934, Sa-P1920, Sa-P1996, Sa-P2003, Sa-2052, Sa-AB77, Sa-AB459, Sa-AB472 were received from JSS Medical College, Mysore, India. The cultures were maintained as glycerol stock at -80 °C.

### 2.3.3. Novobiocin susceptibility testing

Susceptibility to novobiocin was performed for both the standard and clinical isolates by the broth microdilution method according to the CLSI guidelines (Humphries et al., 2018). The antibiotic novobiocin was obtained as DMSO-soluble powder (Sigma-Aldrich (St Louis, MO, USA)) and used for MIC determinations as interpreted in the interpretive susceptibility criteria reported in the appropriate CLSI Tables (CLSI M100 ED31:2021) (Wayne, 2012).

### 2.3.4. Antibacterial evaluation of qsl-304

The doubling dilutions of the test compound qsl-304 were serially aliquoted into each well of a 96-well microplate using 8-points, covering a range from 500-3.9 µg/mL to reach a final assay volume of 100 µL/well. Then, a 10 µL culture suspension of the exponentially growing cells with a seed density of 10<sup>5</sup> CFU/ml was added to each well. The solvent

control (medium with DMSO) and negative controls (medium with culture inoculum; medium with broth) were maintained in all experiments. All independent culture conditions were performed in triplicate. Further, the plates were incubated at 37 °C for 24 h in ambient air and growth was assessed at OD<sub>595</sub> using a microplate reader (iMark, Bio-Rad, Japan). The lowest concentration that completely prevented bacterial growth was categorized as MIC (Wikler, 2006).

### 2.3.5. Time-dependent kill assay

The time-dependent effect of qsl-304 on the growth of the novobiocin resistant clinical isolate *sa*-P2003 was performed using the broth macro-dilution method as per the CLSI guidelines. The exponentially growing cells were used as bacterial inoculum with a 10<sup>5</sup> CFU/ml seed size. The test compound qsl-304 was added to 10 ml of the inoculum suspension to achieve a final concentration of 0.5xMIC, 1xMIC, 2xMIC, 4xMIC, 8xMIC and 16xMIC and maintained at 37 °C in ambient air for 24 h. A growth control (bacterial inoculum without the test compound) was maintained in all independent trials. After 24 h, the aliquots from the inoculum culture were removed at defined time-points (0, 2, 4, 6, 8, 10 and 24 h) and ten-fold serial diluted in saline and the growth was determined by counting the colony-forming units and compared with that of the control (growth media with *Sa*-P2003).

The data was analyzed by evaluating the number of viable cells that yielded  $\Delta(\log_{10}\text{CFU/mL})$  values of  $-1$  (90% killing),  $-2$  (99% killing), and  $-3$  (99.9% killing) at various time-point intervals compared to viable counts at 0 h. The bactericidal activity was calculated as a reduction of at least 99.9% ( $\geq 3 \log_{10}$ ) of the total count of CFU/mL in the original inoculum (Zadrazilova et al., 2015).

### 2.3.6. Frequency of spontaneous resistance to qsl-304

The bacterial strains *Sa*-P2003 and ATCC43300 were cultured in CA-MHB and MHA to examine the frequency of spontaneous resistance to a higher concentration of qsl-304. Briefly, bacterial cultures that reached an exponential phase in CA-MHB were serially diluted to a seed inoculum size of  $\sim 10^9$  cfu/mL and plated onto agar containing 0.5x, 1x, 2x, and 4x MIC of the test compound to calculate the generation and enumeration of resistant mutants. The cultures were also diluted in PBS, and dilutions containing  $\sim 10^2$  cfu/mL were plated onto drug-free agar to enumerate total viable cells. Plates were incubated at 37 °C for 48 h. The experiment was carried out in triplicates, and the negative control (media without qsl-304) was maintained (Huband et al., 2007; Lahiri et al., 2015). After the stipulated time (48 h), the viable cells were counted, and the frequency of spontaneous resistance towards the action of qsl-304 was calculated using the following formulae:

$$\text{Resistance frequency}(fr) = \frac{C_{fur}}{C_{fus}}$$

$C_{fur}$  = CFU/mL of test strain in the presence of qsl-304

$C_{fus}$  = CFU/mL of test strain grown in the absence of qsl-304

### 2.3.7. GyrB inhibition assay

GyrB is the ATP dependent process. The inhibition of the gyrase activity can be indirectly quantified by measuring the ADP generated in the supercoiling process. The gyrase mediated ADP generation was done with *S. aureus* gyrase kit (Inspiralis Ltd., UK). The gyrase enzyme reactions were set as per the manufacturer's instructions. The reaction with a volume of 30  $\mu\text{L}$  was established with the *S. aureus* gyrase assay buffer, relaxed pBR322, gyrase enzyme (1 U), 0.5% DMSO as the solvent. The test compound, qsl-304 was added to the reaction mixture having different concentrations – 0.5X, X, 2X and 4X MIC. Novobiocin was taken as a positive control.

The generation ADP in the presence and the absence of qsl-304 was assessed using the ADP-glo kit (Promega, India). The experiments were conducted as per the manufacturer's instructions. Briefly, 40  $\mu\text{L}$  of ADP-Glo™ reagent was added to the reaction mixture and incubated for 40 min at 37 °C. Subsequently, 50  $\mu\text{L}$  of detection reagent was added to the reaction mixture and re-incubated at 37 °C for 5 min. Luminescence was measured using a microplate reader (BioRad i-Mark, Japan) following the stipulated incubation times. The inhibition of the enzyme activity was evaluated by comparing the luminescence between the control and the qsl-304 treated reactions.

## 2.4. Data analysis

All the *in vitro* experiments were conducted in biological and technical triplicates. All the data obtained were analyzed using GraphPad Prism 8.0.2 software. Dose-response curves were plotted by fitting the inhibition data using a 4-parameter logistic equation.

## 3. Results and discussion

### 3.1. Design and synthesis

The advent of computer-aided drug design reduces the traditional drug discovery process. *De novo* ligand design is a structure-based virtual screening (SBVS) approach to generate a set of target-specific novel chemical hits with desirable activity-enriched profiles. In this regard, the current study aimed to identify potential GyrB inhibitors through a systematic virtual screening process (Figure 1).

The chosen GyrB protein is co-crystallized with an indolinone fragment in its PDB structure (Accession No.:5CPH). This indolinone fragment interacts with the GyrB in its ATP binding site. It interacts with the active site amino acid Asp81 and a crystallographically conserved water molecule like the other potent inhibitors (Mesleh et al., 2016). The docking algorithm was validated with a molecular re-docking procedure. Indolinone was separated from the complex structure and redocked into GyrB. The glide score of the redocked complex was  $-5.68$ , with the RMSD of  $1.23 \text{ \AA}$  between the crystal and computed docked pose of the indolinone fragment. As shown in Figure 2a, binding interaction analysis of the re-docked complex revealed that the N-H group at position 1 and C=O at position 2 participated in

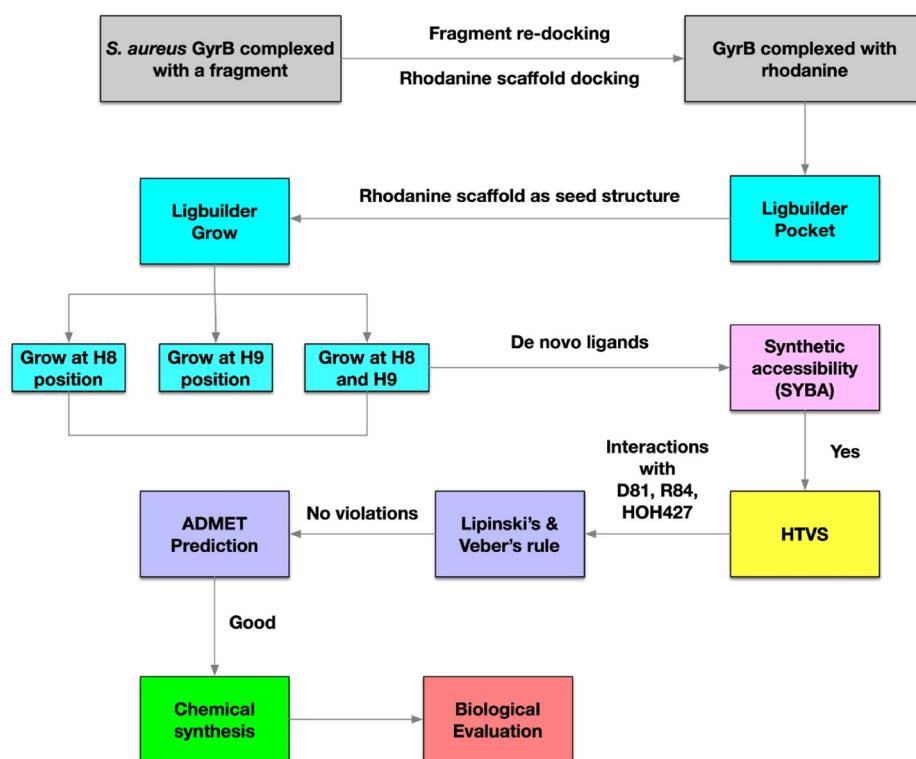


Figure 1. In silico-based lead optimization workflow.

the hydrogen bond network with the carboxylate side chain of Asp81 and crystallographic conserved water molecules, respectively. These results were in coherence with the crystal pose and suggested the consistency of the docking algorithm and force fields used.

After the validation of the docking algorithm, seed structure selection was performed. Seed structure is an integral component of the *de novo* drug design process as it is the starting point of the generation of novel hit molecules. For the current study, rhodanine moiety (2 – thioxothiazolidin – 4 –one) was taken as the building block for the hit generation. Considered to be the "Privileged Scaffold", rhodanine belongs to the family of five-membered multi-heterocycles (FMMH) having an exocyclic sulphur atom (Tomai & Mai, 2009) and owing to its distinct intermolecular interaction pattern, rhodanine scaffold feature in the numerous pharmaceutical molecules (Mendgen et al., 2012). Especially in the post-antibiotic age of antimicrobial resistance several hit molecules with rhodanine scaffold were proved to have effective antimicrobial activity against susceptible and MDR strains of both Gram-negative and Gram-positive bacteria (Maddila et al., 2020). Therefore, the present study was directed toward developing novel hit molecules from rhodanine against *S. aureus* GyrB. Before proceeding with the "growth" of the seed structure, *de novo* ligand design approach uses protein-ligand complex information as the input to construct, and design novel hit molecules. Even though the crystal structures of hit molecules with rhodanine scaffold are available (Werner et al., 2014, 2015), there was no experimentally solved structure of GyrB directly complexed with rhodanine. Hence, to prepare the initial complex structure for *de novo* ligand design, we docked the

rhodanine moiety into GyrB (PDB: 5CPH) and used it for further development and optimization. The docking result shows that the N-H at position three and C=O at position 4 of rhodanine were participating in hydrogen bonding interactions with the side chain of Asp81 and a crystallographic conserved water molecule, respectively (Figure 2b).

The GyrB-rhodanine docked complex was provided as input for LigBuilder. The binding pocket identification and the pharmacophore elements of the input complex structure were identified by running the pocket module of LigBuilder. LigBuilder offers two different strategies (grow and link) to develop novel hit molecules, and in this study, we utilized the grow approach. Two positions of the rhodanine scaffold (N3 and C5) were extensively explored to develop potent antimicrobial derivatives (Werner et al., 2014, 2015; Maddila et al., 2020). In our case, the N3 position of rhodanine participates in the hydrogen bonding interaction with the Asp81, and the two hydrogen atoms at the C5 position were considered for growing the fragment (Figure 3). The two hydrogens at C5 positions were grown separately and simultaneously to obtain structurally diverse rhodanine derivatives. LigBuilder generated a total of 374 hit molecules with the rhodanine scaffold.

Although synthetic accessibility is integrated into the *de novo* ligand design program generating a chemical score, the molecular complexity results in insufficiencies (Selzer et al., 2005)(Sheridan et al., 2014), encouraging us to employ a fragment-based scoring method, SYBA, to evaluate the synthetic accessibility of the generated molecules (Voršilák et al., 2020). The SYBA score is assigned to the molecules derived from the ECFP8 fragments randomly present in the ZINC15 database for ES molecules and Nonpher approach generated compounds

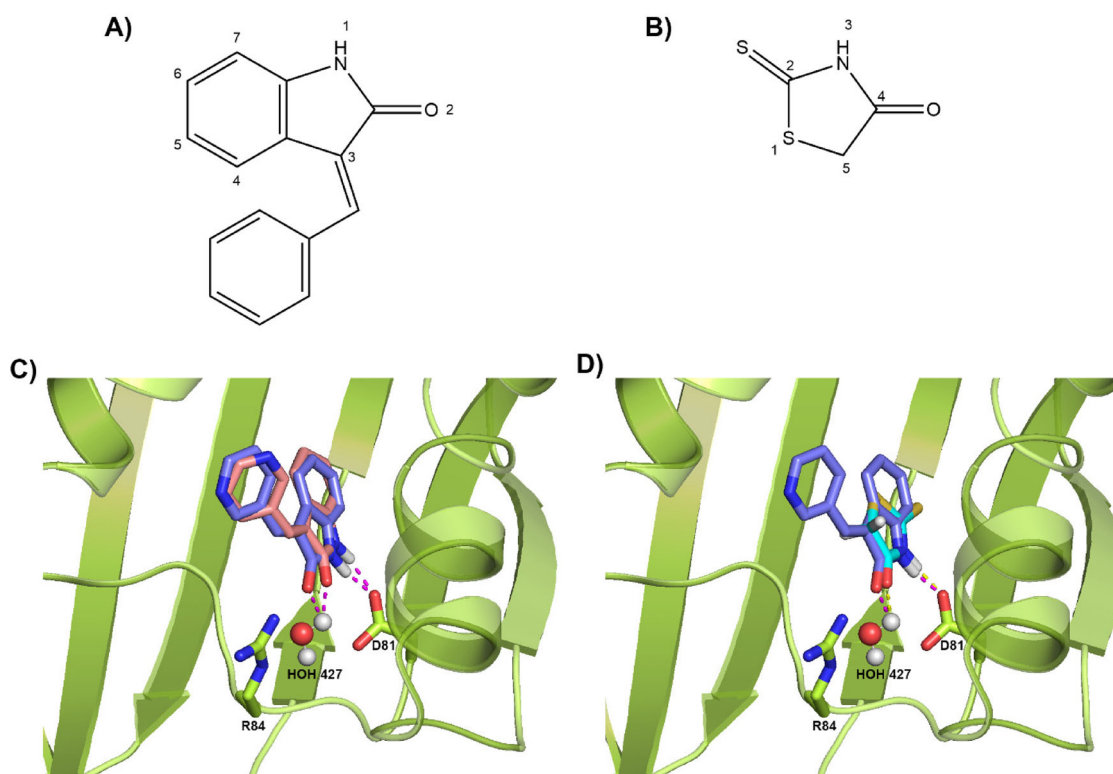


**Figure 2.** A) Structure of the Indolinone fragment B) Structure of rhodanine scaffold used in this study. C) Illustration of redocking of co-crystallized indolinone fragment with GyrB (PDB ID:5CPH). GyrB is represented as a green ribbon. Crystal and docked poses of indolinone were represented as blue and salmon sticks. Hydrogen bonding interactions with Asp 81 and the crystallographically conserved water (427) were designated as pink dotted lines. D) Docking of rhodanine fragment on to GyrB. The green ribbon represents GyrB protein structure. The Blue stick represents the crystal pose of indolinone. Cyan stick represents the docked pose of rhodanine. The pink and yellow dotted line represents the hydrogen bonding interactions of indolinone and rhodanine fragments, respectively.

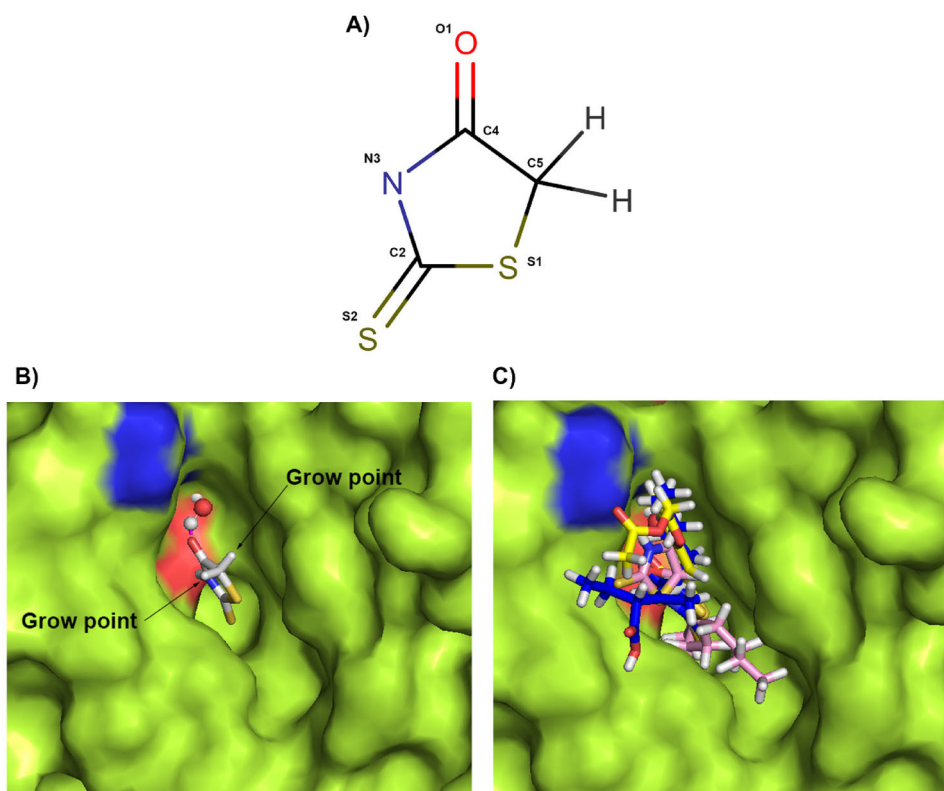


**Figure 3.** Sketch map of the growing operation. (A) Seed Structure (rhodanine scaffold) (B) The docked pose of rhodanine (seed structure) in the ATP binding domain of GyrB. The two hydrogen atoms at C5 positions were labelled as growing points. (C) Representation of molecules grown at two hydrogens at C5 positions of rhodanine individually and simultaneously. The newly developed ligands were represented as sticks.



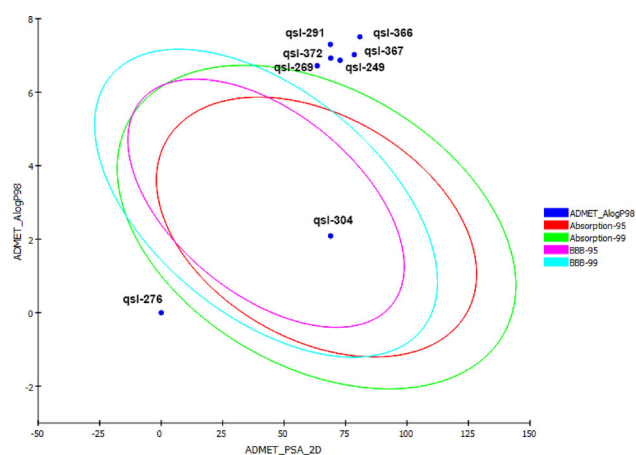
**Table 1.** The hit molecules which passed the Lipinski's rule of five and Veber's rule.

Compound	Lipinski's rule			Veber's rule		
	Molecular weight	Alog P	Hydrogen bond donor	Hydrogen bond acceptor	Rotatable bonds	Molecular polar surface area
qsl-249	484.674	6.867	2	5	8	128.73
qsl-269	455.633	6.717	2	4	7	119.86
qsl-276	580.781	4.404	4	7	10	158.95
qsl-291	472.663	7.298	2	5	10	124.79
qsl-304	283.323	2.089	1	5	4	125.93
qsl-366	463.615	7.505	3	5	7	139.27
qsl-367	480.642	7.021	3	5	10	135.65
qsl-372	479.657	6.927	2	5	7	128.31

**Table 2.** Molecular docking scores of top eight hit molecules.

S.No.	Molecule	GScore	Interacting Residues - Hydrogen bond	Lipophilic EvdW	HBond	Electro	Site
1	qsl-249	-3.826	ARG144	-3.87	-0.35	-0.23	-0.28
2	qsl-269	-3.711	ASP57, H2O	-2.99	-1.32	-0.43	0
3	qsl-276	-5.613	H2O	-3.46	-1.78	-0.37	-0.88
4	qsl-291	-4.096	GLU50, H2O	-3.26	-1.03	-0.33	0
5	qsl-304	-4.911	ASP81, ARG84, H2O	-1.83	-1.33	-0.62	-0.98
6	qsl-366	-4.988		-4.81	-0.66	-0.04	-0.28
7	qsl-367	-4.223	ASP57, ASN54	-3.81	-0.83	-0.06	-0.19
8	qsl-372	-4.073	ASP81	-3.84	-0.35	-0.35	-0.39
9	Novobiocin	-4.724	ASN54, GLU50	-3.9	-1.7	-0.6	0

GScore - Total Glide Score; sum of XP terms. LipophilicEvdW - Lipophilic term derived from hydrophobic grid potential at the hydrophobic ligand atoms. HBond - ChemScore H-bond pair term. Electro - Electrostatic rewards; includes Coulomb and metal terms. Site - Polar interactions in the active site. Polar but non-hydrogen-bonding atoms in a hydrophobic region are rewarded.

**Figure 4.** ADME/T evaluation plot of PSA vs A log P for the eight lead molecules. 99% and 95% confidence limits correspond to intestinal absorption and blood brain barrier models.

for HS molecules. Since the number of stereo centres is limited, compounds with multiple stereo centres are penalized. Hence, the prediction confidence is expressed as a positive SYBA score denotes ES, and a negative score indicates HS. The 374 molecules were analyzed and assigned an SYBA score based on this. The hit molecules having a positive SYBA score were filtered and labelled as ES. Through this filtration process, 374 molecules were reduced to 58 molecules. To further improve the stringency of the hit optimization process, these molecules were looked for in the vital molecular interactions (D81, R84 and HOH427). Among the two pharmacophore features of the previously established GyrB inhibitors, the hydrogen bond-acceptor motif is given primary importance for successfully inhibiting the GyrB ATP activity. The second feature is an aromatic ring forming cation- $\pi$  interaction with Arg-84 and a hydrogen bond with Arg -144 side chain (Mesleh et al., 2016). This process reduced the number of molecules from 57 to 44 hit molecules.

Finally, the drug-likeness and the pharmacokinetic property were evaluated for the 44 molecules. Lipinski's Rule of Five (Lipinski et al., 1997) and Veber's rule (Veber et al., 2002) were assessed for the 44 hit molecules to screen the "druggable" compounds specifically from the oral bioavailability viewpoint. Table 1 lists the Lipinski's and Veber's parameters of eight molecules that followed Lipinski's and Veber's rules. Out of the 44 hit molecules that can be easily synthesized, only 8 obeyed Lipinski's rule of five and Veber. For the eight molecules, logP was within the preferred range of  $<5$ , and the molecular weight was  $\leq 500$  Da depicting good oral bioavailability and membrane permeability. Also, Veber's rule of several rotatable bonds was  $\leq 10$  for the eight-hit molecules, and  $PSA \leq 140 \text{ \AA}$  showcases good intestinal availability. Stereoselectivity of the hit molecules for optimal target binding was evaluated with the number of rotatable bonds (Veber et al., 2002).

Table 2 summarizes the molecular docking scores for the top eight hit molecules and critical interactions. The eight hit molecules made hydrogen bonding interactions predominantly with the critical active site residues, namely D81, R84, G50, R144 and HOH427. Previous studies have established that the commonly found feature of ATPase inhibitors is the hydrogen bond donor-acceptor motif (Mesleh et al., 2016). This is well established for the top hit molecules. While cation- $\pi$  interaction with R84 is considered an essential feature of specific ATPase inhibitors, it was not observed for the top eight hit molecules. Thus, further analysis proceeded with the top hit eight molecules having the acceptable range of docking score and interaction with critical residues, which obeyed Lipinski's and Veber's rule.

As a final screening process, the pharmacokinetic properties of the selected eight hit molecules were performed. Figure 4 shows a biplot figure of the 95% and 99% confidence ellipses of the blood-brain barrier (BBB) and human

**Table 3.** In silico ADME/T prediction of the lead molecules which passed Lipinski's rule and Veber's rule of Drug likeliness.

ADME/ T Parameters	qsl-249	qsl-269	qsl-276	qsl-291	qsl-304	qsl-366	qsl-372
A log p98	6.867	6.717	6.524	7.298	2.089	7.505	6.927
PSA	72.776	63.48		68.829	68.896	80.808	68.896
Aqueous solubility	1	1	1	1	3	0	1
HIA	2	2		3	0	3	2
PPB	0	0	0	0	0	0	0
BBB penetration	4	4		4	3	4	4
Cyp450	0	0	0	0	0	0	0
2D6 binding							
Hepatotoxicity	Toxic	Non-Toxic	Non-Toxic	Toxic	Non-Toxic	Toxic	Non-Toxic
DTP	Toxic	Non-Toxic	Toxic	Toxic	Non-Toxic	Toxic	Non-Toxic
FDA rodent carcinogenicity	Non-carcinogenic	Non-carcinogenic	Non-carcinogenic	Non-carcinogenic	Non-carcinogenic	Non-carcinogenic	Non-carcinogenic
Ames	Non-mutagen	Non-mutagen	Non-mutagen	Non-mutagen	Non-mutagen	Non-mutagen	Non-mutagen
Aerobic biodegradability	Degradable	Degradable	Non-Degradable	Degradable	Degradable	Non-Degradable	Non-Degradable
Skin sensitization	None	Weak	Weak	Weak	Weak	None	Weak
Skin irritating	Mild	Mild	Mild	Mild	Mild	Mild	Mild

A log P98 (atom-based log P) ( $\leq 2.0$  or  $\geq 7.0$ : very low absorption). PSA (polar surface area) ( $> 150$ : very low absorption). Level of aqueous solubility predicted: 0 (extremely low), 1 (very low, but possible), 2 (low), 3 (good), 4 (optimal), 5 (too soluble), 6 (warning: molecules with one or more unknown A log P calculations). HIA (human intestinal absorption), level of human intestinal absorption prediction: 0 (good), 1 (moderate), 2 (poor), 3 (very poor). PPB, plasma protein binding. f BBB (blood brain barrier), level blood brain barrier penetration prediction: 0 (very high penetrate), 1 (high), 2 (medium), 3 (low), 4 (undefined). Prediction cytochrome P4502D6 enzyme inhibition (0: non-inhibitor; 1: inhibitor). h DTP, development toxicity potential. FDA- Food, and drug administration.

intestinal absorption (HIA) properties. Only one of the hit molecules, qsl-304 was within the acceptable ranges of both BBB and HIA. Table 3 depicts the detailed ADME descriptors considered. The hydrophilicity was evaluated by calculating the AlogP value. The values of less than 5 indicate better permeation. In this regard, the hit molecule qsl-304 showed an AlogP value of 2.089, depicting better hydrophilicity and permeation. Polar surface area (PSA) describes the oral bio-availability, which should be  $< 140$ . All the eight molecules were less than the allowed values ranging between 60 – 80. Human intestinal absorption was good only for qsl-304, whereas the other hits had poor or extremely poor absorption values. All the eight molecules could be bound to plasma protein, whereas none of them could penetrate BBB and not inhibit cytochrome p450. Hence all the hit compounds can easily undergo oxidation and hydroxylation during the first phase of metabolism. Among the eight molecules, four (qsl-269, qsl-276, qsl-304 and qsl-372) were non-hepatotoxic and three (qsl-269, qsl-304, qsl-372) were non-DTP toxic. All the eight molecules are non – carcinogenic, non – mutagenic and four hit molecules (qsl-249, qsl-269, qsl-291, qsl-304) were degradable. Considering all these properties, qsl-304 is an ideal candidate for the drug development process. Compared to the positive control, novobiocin ( $-38.11$  kcal/mol), qsl-304 ( $-40.49$  kcal/mol) has enhanced binding energy towards the ATP binding site of *S. aureus* GyrB.

Thus, this systematic screening process identified the *de novo* ligand designed qsl-304 having a higher probability of easy synthesis that makes crucial interactions for significant GyrB inhibition and shows desirable druggable and pharmacokinetics characteristics. It should be noted that qsl-304 makes a hydrogen-bond network with Asp81 and conserved water molecules through the rhodanine moiety. The developed derivative makes hydrogen bond interaction with Arg84, unlike other protein inhibitors that make cation  $\pi$  stacking with Arg84 (Figure 5).

Molecular dynamics simulation studies were performed for GyrB, and qsl-304 docked complexes to understand the interaction stability, conformational behaviour, and binding energy calculations. Figure 6a shows the root mean square deviation (RMSD) of the Protein backbone and the ligand and indicates the docked complex's stability. The RMSD values of the ligand for the last 50 ns of the trajectory centred around 2 Å depicting a stable interaction and minimal conformational change during 300 ns simulation. The hydrogen-bond network of qsl-304 with Asp81 and a conserved water molecule is well established during the simulation duration. Figure 6b shows the ligand atom interaction with Asp81 maintained at as high as 97% and conserved water molecule maintained at 94%, reinforcing the stable interaction of qsl-304 with the crucial residues. A timeline profile of these essential interactions is shown in Figure 6c. The MD simulation results thereby confirm the stable interaction of the hit compound (qsl-304) with GyrB. The MM-GBSA calculations from 61 structures of 300 ns trajectory show the average binding free energy of  $-45.0580$  kcal/mol for the GyrB-qsl304

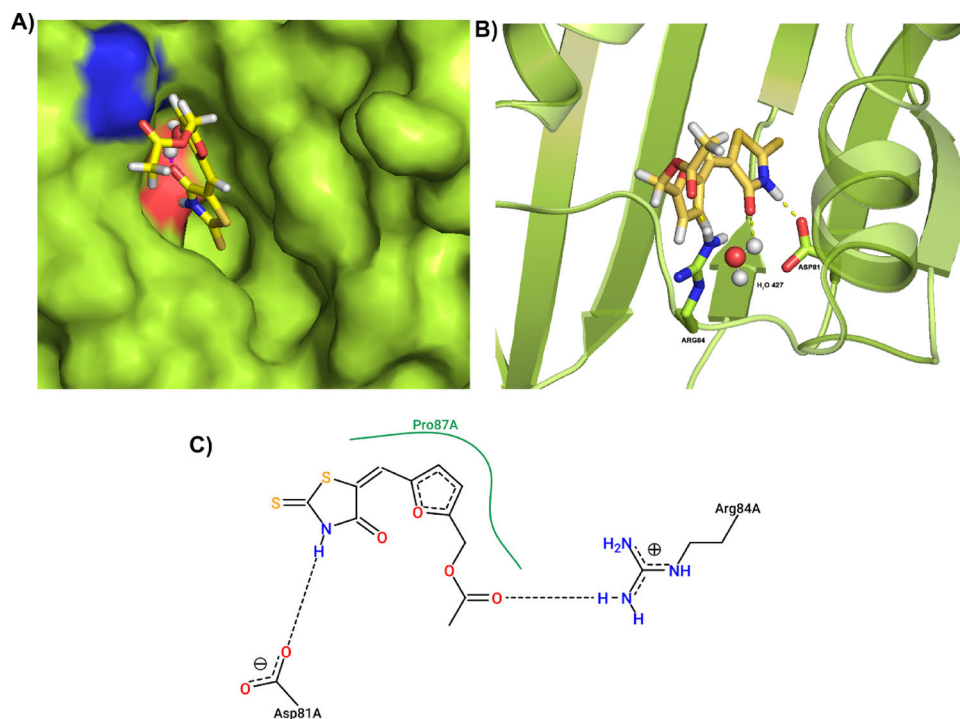


**Figure 5.** Docking pose of qsl-304 in GyrB B ATP domain (a) GyrB is represented as green surface and docked pose of qsl-304 is represented as yellow sticks. (b) GyrB is represented as green ribbon. Active site amino acids were represented as green sticks. The binding pose of qsl-304 is represented as yellow sticks. Hydrogen bonding interaction with the active site residues and the crystallographic water molecules is shown as yellow dotted lines. (c) 2D-interaction map of GyrB-qsl-304.

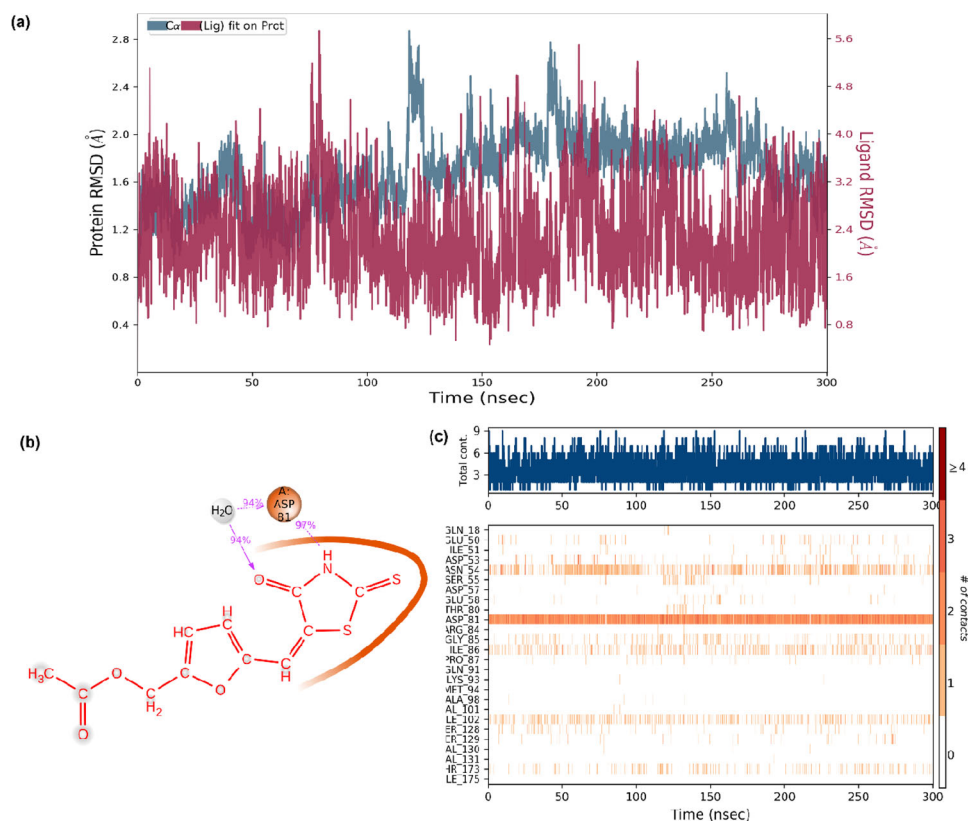


**Figure 6.** Molecular Dynamics Simulation Studies. a) RMSD plot; b) 2D Ligand – atom interaction plot; c) Timeline profile of the ligand residue interactions.

complex. Table S1 compares the average contributing energy terms for the 50 ns simulation for novobiocin and qsl-304.

The top-hit rhodamine scaffold hit compound (qsl-304) was synthesized by the scheme, as shown in Figure 7. The final compound was the yellow solid (1.4 g, 27.5% yield): mp 146 – 147 °C.

### 3.2. Biological efficacy of qsl-304

With time, MRSA has acquired cross-resistance to most classes of antibiotics, thereby increasing the morbidity and mortality rate in hospital-acquired infections (Ventola, 2015). In this accordance, the natural existence of MRSA with cross-resistance to a failed drug, novobiocin, is to be addressed. So, we initially examined the novobiocin profile of the standard strain, *S. aureus* ATCC43300 and the clinical isolates, *Sa*-P1934, *Sa*-P1920, *Sa*-P1996, *Sa*-P2003, *Sa*-2052, *Sa*-AB77, *Sa*-AB459, *Sa*-AB472 (Table S1). Among the considered clinical isolates, novobiocin resistance was observed for *sa*-P1920, *sa*-P1996, *sa*-P1920, *sa*-P1996, *sa*-P1934, *sa*-P2003, *sa*-AB459 and *sa*-AB77. The isolates *sa*-P2052, *sa*-P2040 and *sa*-AB472 were susceptible to novobiocin, whereas it showed a moderate effect on the standard strain, ATCC 43300. For the current study, the novobiocin resistant clinical strain *sa*-P2003 was chosen.

Dose-response (500-3.9 µg/mL) effect of the hit molecule, qsl-304, with rhodanine scaffold was examined in the novobiocin resistant/intermediate *S. aureus* strains (*sa*-P2003 and ATCC 43300) (Figure 8a). The minimum inhibitory concentration of qsl-304 against ATCC43300 and *sa*-P2003 was 6.97 and 31.23 µg/mL, respectively, indicating strain-dependent effects. Several studies have demonstrated rhodanine-derived molecules' antibacterial efficacy against both Gram-positive and Gram-negative pathogens (Maddila et al., 2020). The

presence of a rhodanine scaffold efficiently enhances the antibacterial activity through peptidoglycan inhibition and prevents critical metabolic processes (Tomašić et al., 2010). Studies have also shown the targeted action on DNA gyrase of *E. coli* (Brvar et al., 2012) and *S. aureus* (Werner et al., 2014).

The bactericidal evaluation of qsl304 was tested, and the results are shown in Table 4. The bactericidal activity is defined when the initial inoculum is reduced by 3log<sub>10</sub> CFU/mL. In the current study, the bactericidal effect was not observed until 16x MIC indicating that qsl-304 is bacteriostatic. A maximum of only ~1.5 log reduction was observed in the 16x MIC treatment. While bactericidal action is preferred in most cases, bacteriostatic antibiotics (clindamycin) overcame toxic shock syndrome in *S. aureus* (Pankey & Sabath, 2004). Further studies are underway to explore the extended activities of qsl-304. Time-dependent comparative analysis on the qsl-304 treated and the untreated *S. aureus* cells showed delayed killing kinetics for the qsl-304 treatment, extending generation time to 4.25 h compared to the control having 2.11 h (Figure 8b).

The frequency of spontaneous resistance of qsl-304 was observed for the considered strains ATCC43300 and *sa*-P2003. The data was significant to show a gradual decrease in the colony-forming unit (CFU/ml) on exposure to higher doses (0.5x to 4xMIC) of qsl-304 (Table 5). 4xMIC of qsl304 showed a 60% decrease in cell counts compared to 0.5xMIC.

**Table 4.** Time Kill Kinetics of qsl-304 antimicrobial activity at higher concentrations. <3log<sub>10</sub> fold difference denotes bacteriostatic effect.

Time (h)	Log10 CFU difference					
	0.5X MIC	1X MIC	2X MIC	4X MIC	8X MIC	16X MIC
2	-0.13109	-0.11522	-0.08318	-0.18986	-0.3181	-1.09293
4	-0.18154	-0.32239	-0.28951	-0.49282	-0.65238	-1.38441
6	-0.07488	-0.43306	-0.40239	-0.6479	-0.78419	-1.54983
8	-0.00485	-0.34024	-0.47321	-0.71939	-0.89034	-1.66343
10	-0.00675	-0.22468	-0.41521	-0.63519	-0.7142	-1.54426
24	-0.08665	-0.1568	-0.38371	-0.65963	-0.8006	-1.62342

**Table 5.** Frequency of spontaneous mutation (CFU/mL).

Strains	0.5X MIC	1X MIC	2X MIC	4X MIC
<i>Sa</i> -P2003	$10.9 \times 10^{-1}$	$8.76 \times 10^{-1}$	$7.51 \times 10^{-1}$	$6.58 \times 10^{-1}$
ATCC 43300	$5.21 \times 10^{-1}$	$4.32 \times 10^{-1}$	$2.96 \times 10^{-1}$	$1.91 \times 10^{-1}$

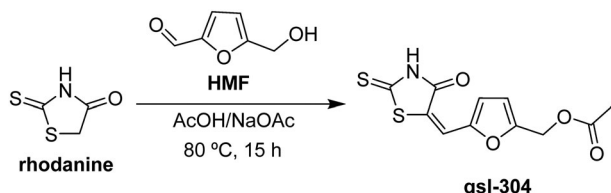


**Figure 7.** Chemical Synthesis Schema.

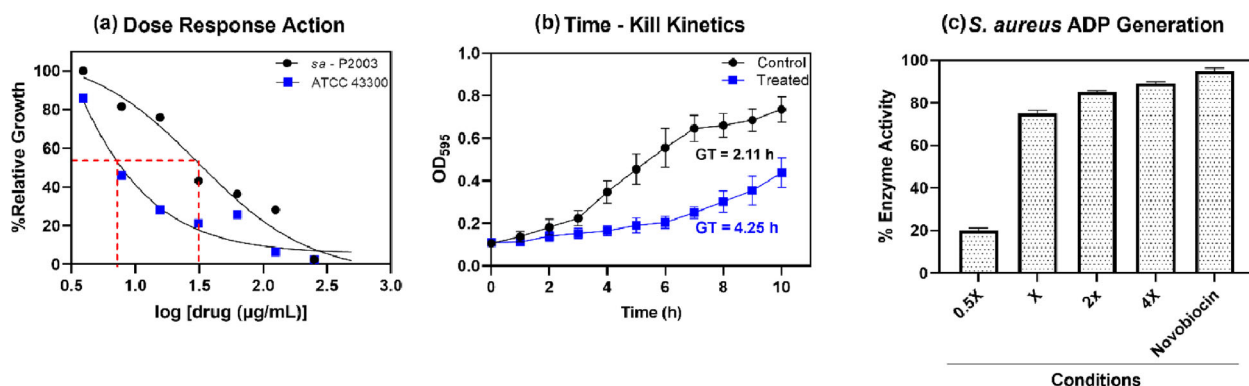


**Figure 8.** a) Dose-Response Curve of qsl-304 against ATCC43300 ( $IC_{50} = 6.97 \mu\text{g/mL}$ ) and *sa*-P2003 ( $IC_{50} = 31.23 \mu\text{g/mL}$ ); b) Time-Kill studies of qsl304 with *Sa*-P2003 having the extended generation time (4.25 h) as compared to the control (2.11 h); c) *S. aureus* gyrase inhibition at varying minimum inhibitory concentrations compared with novobiocin as the positive control, confirming the on-target effect of qsl-304.



Similar effects of qsl-304 were observed in both strains confirming no cross-resistance. The data was compared with the recent work of GlaxoSmithKline (GSK), wherein a series of DNA gyrase inhibitors were identified that invariably developed no cross-resistance with the current topoisomerase-targeting antibacterial agents (Chan et al., 2017).

The on-target effect of qsl-304 against GyrB was evaluated by correlating the ADP generated during the supercoiling process. Figure 8c, depicts the reduction of the enzyme activity in the presence of qsl-304 at varying concentrations. At higher folds of MIC, the enzyme inhibition is evident, which is comparable to Novobiocin. The results obtained correlate well with the aforementioned assays, confirming the qsl-304's gyrase inhibiting activity.

While previous studies (Maddila et al., 2020) were conducted with the standard strains of the MRSA/MSSA, the current study was extended to the clinical isolate of the novobiocin resistance strain and the cross-resistant reference strain ATCC43300. Besides, we showed that the hit compound is less prone to the development of resistance. Previous reports suggest the possibility of rhodanine moiety possessing drug-like molecules having non-specific interactions with off-target effects (Tomašić & Mašić, 2012). With the current study as the background to curb the development of resistance, further studies on cytotoxicity, pharmacophore kinetics and organ-specific drug delivery methods are currently under progress to maximize the targeted effects of the identified hit molecule.

## 4. Conclusion

The alarming increase in antibiotic resistance calls for the need for novel chemical entities to be exploited as antibacterial agents. MRSA is one of the notorious pathogens associated with almost every infection. Thus, there is a pressing need for potent compounds which do not develop resistance. The current report proves a novel GyrB inhibitor, qsl-304, through a systematic *in silico*-based drug designing approach and *in vitro* studies. The identified novel compound can further be exploited as a broad-spectrum antibacterial.

## Acknowledgements

AP, SV, KS, SM, AS, VP, PN and SAP acknowledge SASTRA Deemed to be University, Thanjavur for extending support to use Schrödinger software suite for carrying out *in silico* studies and Professor Sumana MN (Department of Microbiology, JSS Medical College and JSS University, India) for the clinical *S. aureus* strains.







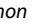

## Disclosure statement

No potential conflict of interest was reported by the authors.

## Funding

The author(s) reported there is no funding associated with the work featured in this article.

## ORCID

Akhila Pudipeddi  <http://orcid.org/0000-0002-0473-5034>  
 Sahana Vasudevan  <http://orcid.org/0000-0002-8817-4704>  
 Karthi Shanmugam  <http://orcid.org/0000-0002-3198-4036>  
 Suma Mohan S  <http://orcid.org/0000-0001-7692-163X>  
 Pothappan Vairaprakash  <http://orcid.org/0000-0001-7181-1028>  
 Prasanna Neelakantan  <http://orcid.org/0000-0003-3025-7598>  
 Alex Stanley Balraj  <http://orcid.org/0000-0003-4474-8830>  
 Adline Princy Solomon  <http://orcid.org/0000-0002-1959-0771>

## Author contributions

Study conception design and project administration: **KS, PN** and **SAP**; Computational data analysis and interpretation of results: **AP, SV, SM, AS** and **KS**; qsl-304 synthesis and characterization: **AP** and **VP**; *in vitro* data acquiring: **AP**; *in vitro* data analysis and interpretation of results: **AP, SV, PN** and **SAP**; Original draft manuscript preparation, writing, reviewing and editing: **AP, SV, KS, PN** and **SAP**. All authors have read and agreed to the published version of the manuscript.

## References

- AbdelKhalek, A., Ashby, C. R., Patel, B. A., Talele, T. T., & Seleem, M. N. (2016). In vitro antibacterial activity of rhodanine derivatives against pathogenic clinical isolates. *Plos One*, 11(10), e0164227–17. <https://doi.org/10.1371/journal.pone.0164227>
- Basarab, G. S., Brassil, P., Doig, P., Galullo, V., Haimes, H. B., Kern, G., Kutschke, A., McNulty, J., Schuck, V. J., Stone, G., & Gowravaram, M. (2014). Novel DNA gyrase inhibiting spiropyrimidinetriones with a benzisoxazole scaffold: SAR and *in vivo* characterization. *Journal of Medicinal Chemistry*, 57(21), 9078–9095.
- Bax, B. D., Murshudov, G., Maxwell, A., & Germe, T. (2019). DNA topoisomerase inhibitors: Trapping a DNA-cleaving machine in motion. *Journal of Molecular Biology*, 431(18), 3427–3449.
- Bisacchi, G. S., & Manchester, J. I. (2015). A new-class antibacterial-almost. Lessons in drug discovery and development: A critical analysis of more than 50 years of effort toward ATPase inhibitors of DNA gyrase and topoisomerase IV. *ACS Infectious Diseases*, 1(1), 4–41. <https://doi.org/10.1021/id500013t>
- Bowers, K. J., Chow, D. E., Xu, H., Dror, R. O., Eastwood, M. P., Gregersen, B. A., Klepeis, J. L., Kolossvary, I., Moraes, M. A., Sacerdoti, F. D., Salmon, J. K., Shan, Y., & Shaw, D. E. (2006). Scalable algorithms for molecular dynamics simulations on commodity clusters. SC '06: *Proceedings of the 2006 ACM/IEEE Conference on Supercomputing*, 43.
- Bozdogan, B., Esel, D., Whitener, C., Browne, F. A., & Appelbaum, P. C. (2003). Antibacterial susceptibility of a vancomycin-resistant *Staphylococcus aureus* strain isolated at the Hershey Medical Center. *Journal of Antimicrobial Chemotherapy*, 52(5), 864–868. <https://doi.org/10.1093/jac/dkg457>
- Brvar, M., Perdih, A., Renko, M., Anderluh, G., Turk, D., & Solmajer, T. (2012). Structure-Based discovery of substituted 4,5'-bithiazoles as novel DNA gyrase inhibitors. *Journal of Medicinal Chemistry*, 55(14), 6413–6426.
- Bush, K., & Jacoby, G. A. (2010). Updated functional classification of  $\beta$ -lactamases. *Antimicrobial Agents and Chemotherapy*, 54(3), 969–976.
- Chan, P. F., Germe, T., Bax, B. D., Huang, J., Thalji, R. K., Bacqué, E., Checchia, A., Chen, D., Cui, H., Ding, X., Ingraham, K., McCloskey, L., Raha, K., Srikannathasan, V., Maxwell, A., & Stavenger, R. A. (2017). Thiophene antibacterials that allosterically stabilize DNA-cleavage complexes with DNA gyrase. *Proceedings of the National Academy of Sciences of the United States of America*, 114(22), E4492–E4500. <https://doi.org/10.1073/pnas.1700721114>
- Chopra, S., Matsuyama, K., Tran, T., Malerich, J. P., Wan, B., Franzblau, S. G., Lun, S., Guo, H., Maiga, M. C., Bishai, W. R., & Madrid, P. B. (2012). Evaluation of gyrase B as a drug target in *Mycobacterium tuberculosis*. *The Journal of Antimicrobial Chemotherapy*, 67(2), 415–421. <https://doi.org/10.1093/jac/dkr449>

- Collin, F., Karkare, S., & Maxwell, A. (2011). Exploiting bacterial DNA gyrase as a drug target: Current state and perspectives. *Applied Microbiology and Biotechnology*, 92(3), 479–497.
- Durcik, M., Lovison, D., Skok, Z., Durante, C., & Tammela, P. (2018). Europe PMC funders group new N -phenylpyrrolamide DNA gyrase B inhibitors: Optimization of efficacy and antibacterial activity. *European journal of medicinal chemistry*, 154, 117–132. <https://doi.org/10.1016/j.ejmech.2018.05.011>
- Friesner, R. A., Murphy, R. B., Repasky, M. P., Frye, L. L., Greenwood, J. R., Halgren, T. A., Sanschagrin, P. C., & Mainz, D. T. (2006). Extra precision glide. Docking and scoring incorporating a model of hydrophobic enclosure for protein-ligand complexes. *Journal of Medicinal Chemistry*, 49(21), 6177–6196. <https://doi.org/10.1021/jm051256o>
- Hardej, D., Ashby, Jr, C. R., Khadtare, N. S., Kulkarni, S. S., Singh, S., Talele, T. T. (2010). The synthesis of phenylalanine-derived C5-substituted rhodanines and their activity against selected methicillin-resistant *Staphylococcus aureus* (MRSA) strains. *European journal of medicinal chemistry*, 45(12), 5827–5832. <https://doi.org/10.1016/j.ejmech.2010.09.045>
- Huband, M. D., Cohen, M. A., Zurack, M., Hanna, D. L., Skerlos, L. A., Sulavik, M. C., Gibson, G. W., Gage, J. W., Ellsworth, E., Stier, M. A., & Gracheck, S. J. (2007). In vitro and in vivo activities of PD 0305970 and PD 0326448, new bacterial gyrase/topoisomerase inhibitors with potent antibacterial activities versus multidrug-resistant gram-positive and fastidious organism groups. *Antimicrobial Agents and Chemotherapy*, 51(4), 1191–1201. <https://doi.org/10.1128/AAC.01321-06>
- Hurley, K. A., Santos, T. M. A., Fensterwald, M. R., Rajendran, M., Moore, J. T., Balmond, E. I., Blahnik, B. J., Faulkner, K. C., Foss, M. H., Heinrich, V. A., Lammers, M. G., Moore, L. C., Reynolds, G. D., Shearn-Nance, G. P., Stearns, B. A., Yao, Z. W., Shaw, J. T., & Weibel, D. B. (2017). Targeting quinolone- and aminocoumarin-resistant bacteria with new gyramide analogs that inhibit DNA gyrase. *MedChemComm*, 8(5), 942–951. <https://doi.org/10.1039/C7MD00012J>
- Johnston, A., & Holt, D. W. (2014). Substandard drugs: a potential crisis for public health. *British Journal of Clinical Pharmacology*, 78(2), 218–243.
- Kohno, S., Yamaguchi, K., Aikawa, N., Sumiyama, Y., Odagiri, S., Aoki, N., Niki, Y., Watanabe, S., Furue, M., Ito, T., Croos-Dabrera, R., & Tack, K. J. (2007). Linezolid versus vancomycin for the treatment of infections caused by methicillin-resistant *Staphylococcus aureus* in Japan. *Journal of Antimicrobial Chemotherapy*, 60(6), 1361–1369. <https://doi.org/10.1093/jac/dkm369>
- Lakhundi, S., & Zhang, K. (2018). Methicillin-resistant *Staphylococcus aureus*: Molecular characterization. *Evolution, and Epidemiology*, 31(4), 1–103.
- Lahiri, S. D., Kutschke, A., McCormack, K., & Alm, R. A. (2015). Insights into the mechanism of inhibition of novel bacteria topoisomerase inhibitors from characterization of resistant mutants of *Staphylococcus aureus*. *Antimicrobial Agents and Chemotherapy*, 59(9), 5278–5287. <https://doi.org/10.1128/AAC.00571-15>
- Lipinski, C. A., Lombardo, F., Dominy, B. W., & Feeney, P. J. (1997). Experimental and computational approaches to estimate solubility and permeability in drug discovery and development settings. *Advanced Drug Delivery Reviews*, 23(1–3), 3–25. [https://doi.org/10.1016/S0169-409X\(96\)00423-1](https://doi.org/10.1016/S0169-409X(96)00423-1)
- Livermore, D. M. (2000). Antibiotic resistance in staphylococci. *International Journal of Antimicrobial Agents*, 16(Suppl 1), S3–S10.
- Maddila, S., Gorle, S., & Jonnalagadda, S. B. (2020). Drug screening of rhodanine derivatives for antibacterial activity. *Expert Opinion on Drug Discovery*, 15(2), 203–229.
- Mani, N., Gross, C. H., Parsons, J. D., Hanzelka, B., Müh, U., Mullin, S., Liao, Y., Grillot, A.-L., Stamos, D., Charifson, P. S., & Grossman, T. H. (2006). In vitro characterization of the antibacterial spectrum of novel bacterial type II topoisomerase inhibitors of the aminobenzimidazole class. *Antimicrobial Agents and Chemotherapy*, 50(4), 1228–1237. <https://doi.org/10.1128/AAC.50.4.1228-1237.2006>
- Mattingly, A. E., Cox, K., Smith, R., Melander, R. J., Ernst, R. K., & Melander, C. (2020). Screening an established natural product library identifies secondary metabolites that potentiate conventional antibiotics. *ACS Infectious Diseases*, 6(10), 2629–2640. <https://doi.org/10.1021/acsfeddis.0c00259>
- Mendgen, T., Steuer, C., Klein, C. D. (2012). Privileged scaffolds or promiscuous binders: a comparative study on rhodanines and related heterocycles in medicinal chemistry. *Journal of medicinal chemistry*, 55(2), 743–753. <https://doi.org/10.1021/jm201243p>
- Mesleh, M. F., Cross, J. B., Zhang, J., Kahmann, J., Andersen, O. A., Barker, J., Cheng, R. K., Felicetti, B., Wood, M., Hadfield, A. T., Scheich, C., Moy, T. I., Yang, Q., Shotwell, J., Nguyen, K., Lippa, B., Dolle, R., & Ryan, M. D. (2016). Fragment-based discovery of DNA gyrase inhibitors targeting the ATPase subunit of GyrB. *Bioorganic & Medicinal Chemistry Letters*, 26(4), 1314–1318. <https://doi.org/10.1016/j.bmcl.2016.01.009>
- Pankey, G. A., & Sabath, L. D. (2004). Clinical relevance of bacteriostatic versus bactericidal mechanisms of action in the treatment of gram-positive bacterial infections. *Clinical Infectious Diseases: An Official Publication of the Infectious Diseases Society of America*, 38(6), 864–870.
- Patel, B. A., Ashby, Jr, C. R., Hardej, D., Talele, T. T. (2013). The synthesis and SAR study of phenylalanine-derived (Z)-5-arylmethylidene rhodanines as anti-methicillin-resistant *Staphylococcus aureus* (MRSA) compounds. *Bioorganic & medicinal chemistry letters*, 23(20), 5523–5527. <https://doi.org/10.1016/j.bmcl.2013.08.059>
- Purnapatre, K. P., Rao, M., Pandya, M., Khanna, A., Chaira, T., Bambal, R., Upadhyay, D. J., & Masuda, N. (2018). In vitro and in vivo activities of DS86760016, a novel leucyl-tRNA synthetase inhibitor for Gram-negative pathogens. *Antimicrobial Agents and Chemotherapy*, 62(4), e01987-17. <https://doi.org/10.1128/AAC.01987-17>
- Ray, P., Gautam, V., Singh, R. (2011). Methicillin-resistant *Staphylococcus aureus* (MRSA) in developing and developed countries: implications and solutions. *InRegional Health Forum* 15(1), 74–82.
- Rice, L. B. (2006). Antimicrobial resistance in gram-positive bacteria. *American Journal of Infection Control*, 34(5 Suppl 1), S11–S73. <https://doi.org/10.1016/j.ajic.2006.05.220>
- Rice, L. B. (2008). Federal funding for the study of antimicrobial resistance in nosocomial pathogens: No ESKAPE. *The Journal of Infectious Diseases*, 197(8), 1079–1081. <https://doi.org/10.1086/533452>
- Rosatella, A. A., Simeonov, S. P., Frade, R. F. M., & Afonso, C. A. M. (2011). 5-Hydroxymethylfurfural (HMF) as a building block platform: Biological properties, synthesis and synthetic applications. *Green Chemistry*, 13(4), 754–793. <https://doi.org/10.1039/c0gc00401d>
- Sareena, C., & Vasu, S. T. (2020). Identification of 4-diphenylamino 3-iodo coumarin as a potent inhibitor of DNA gyrase B of *S. aureus*. *Microbial Pathogenesis*, 147(July), 104387.
- Sastry, G. M., Adzhigirey, M., Day, T., Annabhimoju, R., & Sherman, W. (2013). Protein and ligand preparation. Parameters, protocols, and influence on virtual screening enrichments. *Journal of Computer-Aided Molecular Design*, 27(3), 221–234. <https://doi.org/10.1007/s10822-013-9644-8>
- Savage, V. J., Charrier, C., Salisbury, A. M., Moyo, E., Forward, H., Chaffer-Malam, N., Metzger, R., Huxley, A., Kirk, R., Uosis-Martin, M., Noonan, G., Mohmed, S., Best, S. A., Ratcliffe, A. J., & Stokes, N. R. (2016). Biological profiling of novel tricyclic inhibitors of bacterial DNA gyrase and topoisomerase IV. *The Journal of Antimicrobial Chemotherapy*, 71(7), 1905–1913. <https://doi.org/10.1093/jac/dkw061>
- Selzer, P., Roth, H.-J., Ertl, P., & Schuffenhauer, A. (2005). Complex molecules: do they add value? *Current Opinion in Chemical Biology*, 9(3), 310–316.
- Sheridan, R. P., Zorn, N., Sherer, E. C., Campeau, L.-C., Chang, C., Cumming, J., Maddess, L. M., Nantermet, P. G., Sinz, C. J., & O'Shea, P. D. (2014). Modeling a crowdsourced definition of molecular complexity. *Journal of Chemical Information and Modeling*, 54(6), 1604–1616. <https://doi.org/10.1021/ci5001778>
- Solapure, S. P. S. H., Mukherjee, K., Nandi, V., Waterson, D., Shandil, R., Balganes, M., Sambandamurthy, V. K., Raichurkar, A. K., Deshpande, A., Ghosh, A., Awasthy, D., Shanbhag, G., Sheikh, G., McMiken, H., Puttur, J., Reddy, J., Werngren, J., Read, J., ... Panduga, V. (2014). Optimization of pyrrolamides as mycobacterial gyrb ATPase inhibitors: Structure-activity relationship and in vivo efficacy in a mouse model of tuberculosis. *Antimicrobial Agents and Chemotherapy*, 58(1), 61–70. <https://doi.org/10.1128/AAC.01751-13>

- Tiz, D. B., Skok, Ž., Durcik, M., Tomašič, T., Mašič, L. P., Ilaš, J., Zega, A., Draskovits, G., Révész, T., Nyerges, Á., Pál, C., Cruz, C. D., Tammela, P., Žigon, D., Kikelj, D., & Zidar, N. (2019). An optimized series of substituted N-phenylpyrrolamides as DNA gyrase B inhibitors. *European Journal of Medicinal Chemistry*, 167, 269–290. <https://doi.org/10.1016/j.ejmech.2019.02.004>
- Tomai, T., & Mai, L. P. (2009). Rhodanine as a privileged scaffold in drug discovery. *Current Medicinal Chemistry*, 16, 1596–1629.
- Tomašič, T., & Mašič, L. (2012). Rhodanine as a scaffold in drug discovery: a critical review of its biological activities and mechanisms of target modulation. *Expert Opinion on Drug Discovery*, 7(7), 549–560.
- Tomašič, T., & Mašič, L. (2014). Prospects for developing new antibacterials targeting bacterial type IIA topoisomerases. *Current Topics in Medicinal Chemistry*, 14(1), 130–151.
- Tomašič, T., Zidar, N., Kovac, A., Turk, S., Simcic, M., Blanot, D., Müller-Premru, M., Filipic, M., Grdadolnik, S. G., Zega, A., Anderluh, M., Gobec, S., Kikelj, D., & Peterlin Masic, L. (2010). 5-benzylidenethiazolidin-4-ones as multitarget inhibitors of bacterial mur ligases. *ChemMedChem*, 5(2), 286–295. <https://doi.org/10.1002/cmdc.200900449>
- Veber, D. F., Johnson, S. R., Cheng, H. Y., Smith, B. R., Ward, K. W., Kopple, K. D. (2002). Molecular properties that influence the oral bioavailability of drug candidates. *Journal of medicinal chemistry*, 45(12), 2615–2623. <https://doi.org/10.1021/jm020017n>
- Ventola, C. L. (2015). The antibiotic resistance crisis: causes and threats. *P & T: A Peer-Reviewed Journal for Formulary Management*, 40(4), 277–283.
- Voršilák, M., Kolář, M., Čmelo, I., & Svozil, D. (2020). SYBA: Bayesian estimation of synthetic accessibility of organic compounds. *Journal of Cheminformatics*, 12(1), 1–13. <https://doi.org/10.1186/s13321-020-00439-2>
- Wang, R., Gao, Y., & Lai, L. (2000). LigBuilder: A multi-purpose program for structure-based drug design. *Journal of Molecular Modeling*, 6(7–8), 498–516. <https://doi.org/10.1007/s0089400060498>
- Wayne, P. A. (2012). *CLSI Methods for antimicrobial susceptibility testing of anaerobic bacteria: approved standard-CLSI document M11-A8*. Clinical and Laboratory Standards Institute.
- Werner, M. M., Li, Z., & Zauhar, R. J. (2014). Computer-aided identification of novel 3,5-substituted rhodanine derivatives with activity against *Staphylococcus aureus* DNA gyrase. *Bioorganic & Medicinal Chemistry*, 22(7), 2176–2187.
- Werner, M. M., Patel, B. A., Talele, T. T., Ashby, C. R., Li, Z., & Zauhar, R. J. (2015). Dual inhibition of *Staphylococcus aureus* DNA gyrase and topoisomerase IV activity by phenylalanine-derived (Z)-5-arylmethylene rhodanines. *Bioorganic & Medicinal Chemistry*, 23(18), 6125–6137.
- Wikler, M. A. (2006). Methods for dilution antimicrobial susceptibility tests for bacteria that grow aerobically: approved standard. *CLSI (NCCLS)*, 26, M7–A7.
- Wong, E., & Rab, S. (2014). Tedizolid phosphate (Sivextro): A second-generation oxazolidinone to treat acute bacterial skin and skin structure infections. *P & T: A Peer-Reviewed Journal for Formulary Management*, 39(8), 555–559.
- Zadrazilova, I., Pospisilova, S., Masarikova, M., Imramovsky, A., Ferriz, J. M., Vinsova, J., Cizek, A., & Jampilek, J. (2015). Salicylanilide carbamates: Promising antibacterial agents with high in vitro activity against methicillin-resistant *Staphylococcus aureus* (MRSA). *European Journal of Pharmaceutical Sciences: Official Journal of the European Federation for Pharmaceutical Sciences*, 77(June), 197–207.